A joystick demonstrator for three dimensional magnetic Hall sensors

T. Brouwer
F. Voordenhout

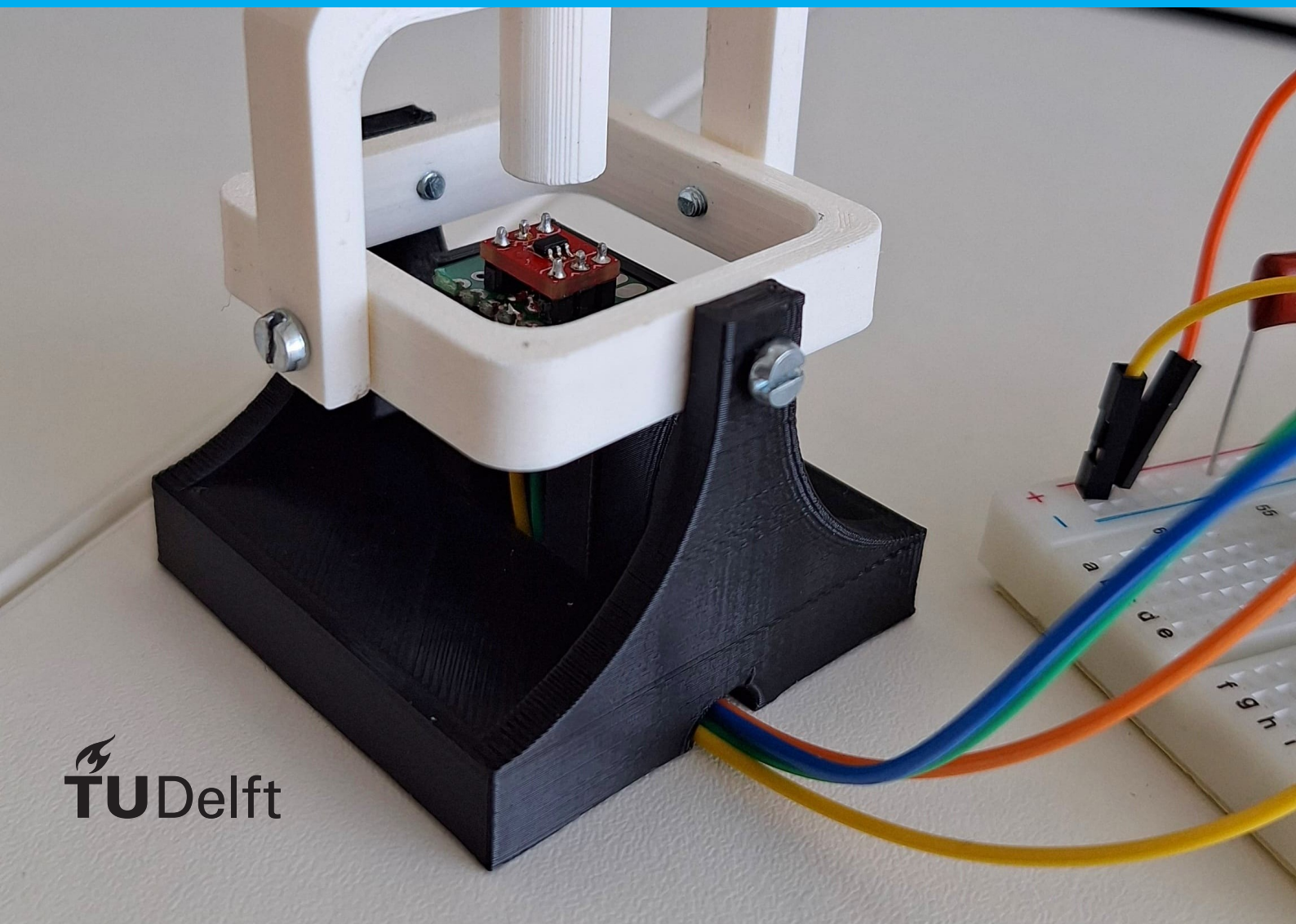

TU Delft

A joystick demonstrator for three dimensional magnetic Hall sensors

T. Brouwer
F. Voordenhout

Student names: Tycho Brouwer 5866642
Francis Voordenhout 5782767

Jury members: Dr. İlke Ercan
Dr. Karen Dowling
Msc. Jacopo Ruggeri

Date: July 9, 2025

TU Delft

Abstract

As novel three dimensional Hall sensors are being developed, it is important to be able to demonstrate their working principles and applications to other researchers and potential investors. One such application is seen in joysticks, which are more durable and reliable when they are made with Hall sensors compared to traditional potentiometer joysticks. In order to develop the joystick, readout mechanisms for multiple commercial Hall sensors are developed first. A joystick design configuration and permanent magnet are selected based on requirements and magnetic field simulations. The joystick is 3D printed and a demonstration screen showing the position of the stick and a moving ball is developed. The joystick has a delay of 9 ms, a maximum pitch of 61°, a resolution higher than 1° and an average error of 2.4° for the pitch and 1.59° for the rotation angle. However, this error may be due to the way the angle was physically measured, rather than errors in the measured magnetic field. Overall, the resulting joystick prototype functions more than sufficiently as a demonstrator.

Preface

This thesis was written as a part of the Bachelor Graduation Project of Electrical Engineering at the TU Delft. We built a working joystick from just a sensor, an Arduino and some basic components and learned many things along the way. We would like to express our gratitude to dr. Karen Dowling for proposing this project and being an awesome supervisor. Furthermore, we want to thank dr. Leon Abelmann for the feedback and discussions on our project and for helping us select a magnet. We would also like to express our gratitude toward Peter Nagy for taking the time to explain some 3D printing principles to us, and toward Lukasz Pakula for helping us use the 3D printer and providing wires and components. We also want to thank Lex Pardon for helping us solder the Melexis sensor and discussing the sensor readout with us. Lastly, we would like to thank Angelie Repriels and Toby van Hooff for being great group members and friends.

Contents

1 Introduction

Joysticks have existed for over a century and have been growing in popularity, especially in the past few decades. They are most commonly associated with the gaming industry, including products like gamepads, arcade joysticks and flight simulator joysticks. However, joysticks may also be used to control wheelchairs [1], to control robots [2], to perform robotic surgery [3] and to control heavy machinery [4]. This shows that development of joysticks no longer benefits just the entertainment industry, but also many control applications. There are currently two main technologies used to read out the position of a joystick: potentiometers and Hall effect magnetic sensors. Most commercial joysticks that are on the market right now use potentiometers.

Potentiometer joysticks

A potentiometer uses a resistive block with a voltage applied across it, and a movable wiper that changes position. For joysticks, this resistive block has a ring shape, as seen in Figure 1.1. When the position of the wiper changes, there is a change in resistance between the wiper and either the ground or the supply terminal. In a circuit, this can be seen as a voltage divider, where one resistance gets smaller and the other gets larger as the wiper changes position. Hence, the voltage on the tap changes depending on the position of the wiper. As the wiper slides over the resistive block, friction slowly wears it down over time.

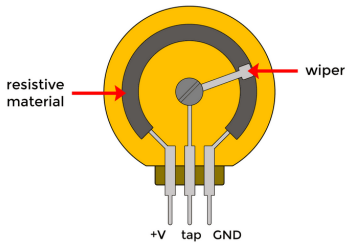

Figure 1.1: Potentiometer structure [5].

The internal structure of a commercial potentiometer joystick can be seen in Figure 1.2. The centre of the wiper must be connected to the rotating ball on the joystick. Two orthogonal potentiometers are used to read out both angles of the movement. These correspond to the angles in spherical coordinates, with a constant radius.

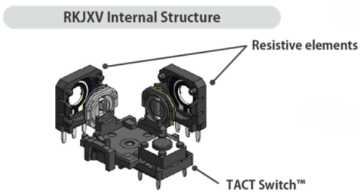

Figure 1.2: Internal structure of traditional potentiometer joystick [6].

Due to wearing, this joystick has a lifetime of two million cycles [6] and is commonly used in game controllers. The lifetime of the joystick will then generally determine the lifetime of the entire controller, meaning shorter lifetimes may lead to more electronic waste. This type of waste is often not formally collected or recycled, and if the lead in electronics leaks into the environment, it can have adverse health effects, especially for children [7]. Furthermore,

users have to buy a new controller every few years, making them more expensive over a longer period of time as compared to a longer lasting joystick. Furthermore, the wearing causes the potentiometer to give inaccurate output, which results in joystick drift. When this happens, the joystick either measures a movement, when the stick is really in its zero position, or the movement measured has an offset compared to the actual stick movement. For these reasons, other joystick technologies like Hall effect sensors may be better suited in situations that require higher reliability and longer lifetime.

Utilizing 3D Hall sensors in joystick applications

Many of the shortcomings of the potentiometer joysticks can be improved by replacing the potentiometers with Hall sensors. Whereas traditional potentiometer joysticks have mechanical contacts, Hall effect joysticks can be made contact free. This improves their lifetime, as mechanical friction makes components prone to wearing.

The following part of this subsection is based on data from Texas Instruments [8], [9]. A 3D Hall effect sensor is a device capable of detecting the magnetic field vector components along three axes x, y, and z. This makes it particularly well-suited for joystick applications, where a magnet moves relative to the sensor across multiple degrees of freedom. In a typical implementation, a permanent magnet is attached to the movable part of the joystick, while the 3D Hall sensor remains stationary on the circuit board. As the joystick is manipulated, tilted in different directions, or pressed, the position and orientation of the magnet change relative to the sensor. These movements result in corresponding changes in the surrounding magnetic field, which the sensor is able to measure.

Because a 3D Hall sensor can separately measure the magnetic field strength along the x, y, and z axes, it can uniquely identify the position of the magnet in three-dimensional space. This allows each physical position of the joystick to produce a distinct magnetic field signature, resulting in a unique sensor readout. The sensor outputs this information as analogue or digital signals that can be interpreted by a microcontroller to determine the joystick's exact position and motion. There are multiple possible configurations for placing the sensor and magnet in a joystick, such as using a spherical, a cylindrical or an axial ring magnet, from left to right in Figure 1.3, the two most right ones are a more complex implementation of a 3D and 1D Hall sensor.

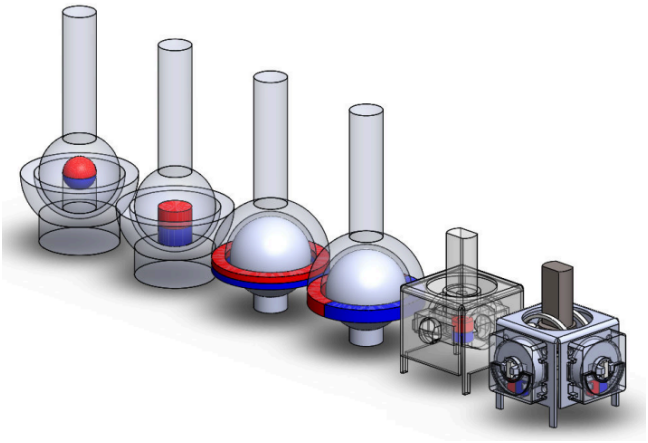

Figure 1.3: Possible configurations for a joystick with a 3D Hall sensor [8]

A Hall sensor is designed to operate within a specific range of magnetic field strengths. If the magnetic field is too weak, the sensor may not detect any significant change compared to the electrical noise, resulting in poor resolution or inaccurate readings. On the other hand, if the magnetic field is too strong, the sensor could become saturated, rendering it unable to distinguish between different positions of the magnet.

The joystick is best represented in a spherical coordinate system, seen in Figure 1.4, because the movement of the joystick is spherical. The joystick stick points in the $\hat{z}$ direction, with a rotation point at $(0,0,0)$, the magnet is placed somewhere at $(0,0,-z)$. The pitch angle of the joystick is represented by θ and the rotation angle by ϕ. To convert the output of the sensor to a rotation angle one can use the following formula.

$$\text{rotation angle} = \phi = \arctan(\frac{y}{x}) = \arctan(\frac{\frac{Y\_measured - Y\_Centre}{Y\_Max - Y\_Centre}}{\frac{X\_measured - X\_Centre}{X\_Max - X\_Centre}}) \tag{1.1}$$

However, the results of this formula only lie between -90° and 90°. In the case that x is negative, an additional 180° must be added to obtain the correct angle. This means the sign of the x field must be checked before applying the

formula. The joystick pitch can be calculated as long as the maximum pitch is known.

$$\text{pitch angle} = \theta = \text{Pitch}_{max} \cdot \left(\frac{x^2 + y^2}{x_{max}^2 + y_{max}^2}\right) \tag{1.2}$$

However, these equations only use the x and y coordinates but the sensor also has a z-axis output. The third axis can be used to obtain a more accurate calculation of theta.

$$\theta = \arctan\left(\frac{\sqrt{x^2 + y^2}}{z}\right) \tag{1.3}$$

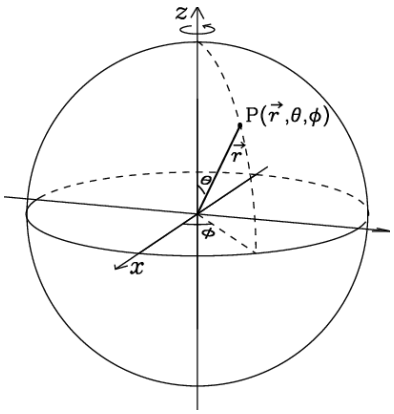

Figure 1.4: The spherical polar coordinate system

When the joystick returns to its neutral or zero position, ideally, the sensor should produce a corresponding zero or baseline output, indicating no movement. In the ideal case any offset is corrected in the calibration of the sensor with a zero gauss chamber. However, in practice, this is rarely the case. Stray magnetic fields (including earth's field), small mechanical misalignments, inconsistencies in the positioning of the magnet, and variations in the manufacturing process can all contribute to slight deviations in the sensor output, even when the joystick is physically centred.
To address these imperfections, joystick systems commonly implement a "dead zone", a small region around the zero position in which any sensor output is ignored or interpreted as zero. This prevents minor fluctuations or noise from causing unintended input, and ensures a more stable and predictable behaviour when the joystick is at rest. The size of the dead zone is typically chosen based on the expected variation range and the precision requirements of the application.

In addition to applying a dead zone, the joystick must also be calibrated in order to provide meaningful input to software or control systems. Calibration involves identifying the full range of motion by determining the minimum and maximum values of the sensor's output in each direction. This allows the system to normalize or map the raw sensor data into a consistent input range, such as from -1 to 1, depending on the desired resolution and data format.

3D Hall sensors working principle

In order to properly integrate 3D Hall sensors into a joystick, some basic understanding of their working principle is needed. A Hall-effect sensor is a type of magnetic sensor that produces an output voltage in response to an incident magnetic field, a phenomenon known as the Hall effect. This magnetic field should be out of plane with the device, ideally orthogonal to it. Hall effect sensors are typically made of semiconductor material, where n-type material is favoured. The output Hall voltage, V_H, depends on charge carrier mobility, and electron mobility is always higher than hole mobility [10]. In metallic conductors, the Hall effect can be sensed as well, though the effect is much larger in semiconductors [11]. Figure 1.5 (left) shows a side view of the way a Hall device can be constructed using semiconductor material. The n-well is surrounded by a p-type substrate, and the contacts are made of n-type as well, only higher doped than the well. In general, a relatively low doped material is used, as the sensitivity of the device drops as the doping concentration increases.

A 1D Hall sensor commonly has four contacts, as shown in Figure 1.5 (right). Two contacts on one of the diagonals are used for the electrical energy supply, and the other two are used for the measurement of V_H. Current flows from one contact diagonally over the plate to another contact. In the presence of a magnetic field, the Lorentz Force will deflect the moving charge carriers. This deflection results in a voltage difference, V_H, which can be measured using the other two contacts. The relative size of the contact to the whole device is very important [12]. If the contact is small, too large a resistance in the connection between the contact and the rest of the device may occur. On the other hand, too

large a contact will short circuit either the bias current or V_H.

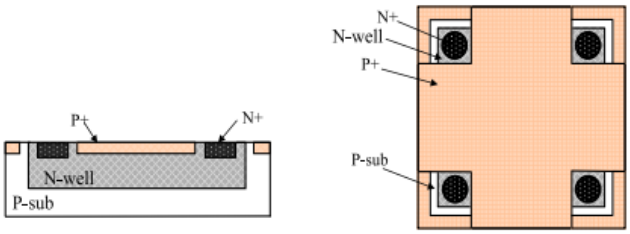

Figure 1.5: 1D Hall device

There are numerous benefits of using Hall effect sensors [10],[12]. The architecture of the device is rather simple, allowing easy manufacturing and ensuring low costs. The construction is an easily repeatable operation, and it is highly similar to microelectronics fabrication. Once constructed, the devices prove to be quite robust as well. Whereas a 1D Hall sensor can only sense the field strength in one direction, many applications require the field to be known in two or three dimensions. This is where 3D Hall sensors come into play. Although they tend to have a lower signal to noise ratio and more crosstalk than one dimensional Hall sensors, 3D Hall sensors are very suitable for joystick applications.

A 3D Hall sensor can be made by integrating three 1D sensors. Such a sensor will consist of one Planar Hall Device (PHD) and two Vertical Hall Devices (VHD). They detect magnetic fields perpendicular and parallel to the device, respectively. Planar Hall Devices work the same as the 1D Hall device described above. Vertical Hall Devices are a bit more complicated, as they have to measure parallel magnetic fields. In Figure 1.6, the PHD measures the magnetic field in the z direction, while the VHDs measure the field in the x and y direction.

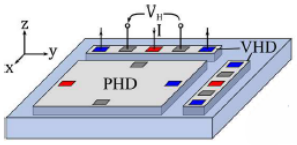

Figure 1.6: Structure of a 3D Hall sensor consisting of two VHDs and one PHD [13].

Generally, the sensitivity of the PHD is six times higher than that of the VHD [14]. Furthermore, both devices have a large offset. In PHDs this offset can be cancelled by a technique called current spinning, which involves quickly changing the direction of the current through the device. The offset in VHDs is caused by the Junction Field Effect, and can be reduced by changing the structure of the P-well as compared to traditional VHDs, such that it has a smaller doping profile in the middle [15].

While combining a PHD with VHDs is currently the most commonly used configuration to measure all three fields, other types of design are possible. Proposals include a cube [16], a hexagon [17] and a combination of planar Hall devices [18], each of which have their own shortcomings. A promising proposal involves an inverted pyramid structure, a CMOS compatible 3D Hall sensor that has similar sensitivities in each direction [13] and can be current spun to remove offset [19]. However, this Hall sensor configuration is still under development and not ready to be used commercially.

Magnetic fields of a permanent magnet

A permanent magnet is a ferromagnetic material that has been magnetized, which means that equal spins within the material are aligned in parallel [20]. Spin, in this case, can be seen as the intrinsic magnetic moment of elementary particles, such as electrons. Permanent magnets are easy to put in moving parts of the joystick and can produce strong fields. This strength of the magnetic field, measured at the sensor, is influenced by several factors. First is the intrinsic strength of the magnet, which depends on its material composition. Additionally, the geometry of the magnet, such as its size and shape, also affects the field distribution. Perhaps most critically, the distance between the magnet and the sensor plays a significant role. As the magnet moves closer to the sensor, the magnetic field at the sensing point increases very quickly. However, as demonstrated by Figure 1.7b, the magnetic field produced by a permanent magnet is predominately non-uniform, except for a narrow region along the symmetry axis of the magnet. The magnetic flux density on the symmetry axis of an axially magnetised cylinder magnet is given by Equation 1.4 [21], where B_r is the magnet remanence field, z the distance from a pole face on the symmetrical axis, D the thickness of the cylinder and R the radius of the cylinder, as shown in Figure 1.7a.

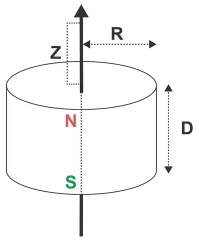

(a) Cylinder magnet [21]

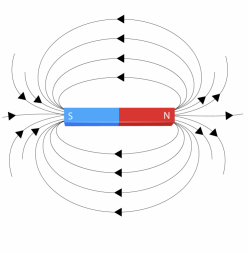

(b) Magnetic field of a permanent magnet [22]

Figure 1.7: Structure and magnetic field of a permanent magnet

$$\mathbf{B}_z = \hat{\mathbf{z}} \cdot \frac{B_r}{2} \cdot \left(\frac{D+z}{\sqrt{R^2+(D+z)^2}} - \frac{z}{\sqrt{R^2+z^2}} \right) \tag{1.4}$$

However, if the distance between the permanent magnet and the sensor is much larger than the dimensions of the magnet, it can be considered a magnetic dipole, and equations simplify significantly . On the axis, the magnetic field is then as follows [23]:

$$\mathbf{H} = \hat{\mathbf{z}} \cdot \frac{m}{2\pi |z|^3} \tag{1.5}$$

With m the magnetic moment and z the distance to the dipole. The strength of the magnetic field can thus be varied strongly by changing the distance between the magnet and the sensor. As demonstrated by Figure 1.8, as distance to the sensor z increases, the magnetic field strength decays rapidly, while at the surface of the magnet the field is strong and changes non-linearly. A permanent magnet can provide very strong magnetic fields compared to electromagnets, ranging from $0.1T$ to $1T$, depending material and size [22].

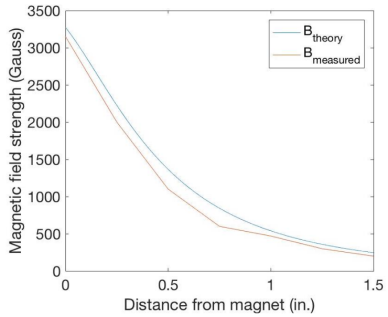

Figure 1.8: Plot of magnetic field strength vs distance from a magnet pole for a single N52-neodymium magnet [24, Figure 8]

1.1. Problem definition

The development of 3D Hall sensors, the pyramid sensor in particular, is a great feat of innovation. However, it is quite difficult to present the performance of just the sensor to potential customers or stakeholders. Integrating such a sensor into an application which demonstrates its capabilities will give a quicker insight into how it performs. It would be ideal if this demonstration is interactive, as this draws more attention than a simple poster or unmoving prototype would. Since joysticks are an important application of 3D Hall effect sensors and can easily be made interactive, they are a clear choice for a demonstrator.

Hall sensor joysticks are superior over potentiometer joysticks in terms of durability, sustainability and reliability. Naturally, a 3D Hall sensor that is easy to manufacture whilst also having high sensitivity and low offset would be preferred in such an application. Once the pyramid sensor is fully developed, a joystick could be a great way to demonstrate its capabilities. However, its read out interface is still a work in progress. Hence, developing a joystick that works with a commercial 3D Hall sensor will already demonstrate the potential of Hall sensor joysticks. Furthermore, once the pyramid sensor is fully developed, it will be relatively easy to replace the commercial sensors with it.

1.2. Thesis synopsis

The main topic of this thesis to describe the design process of a joystick based on a 3D hall sensor and a demonstration showing the workings of the joystick. The structure is as follows: chapter 2 lists the requirements for the whole joystick design and demonstration. The design process is described in chapter 3, this includes the available sensors, how the

field measurement corresponds to the angle of the joystick, different mechanical joystick designs, what magnet to select and considerations for the demonstration. Then chapter 4 shows the final results achieved for the whole system. Possible flaws are discussed in chapter 5. Finally, chapter 6 gives a conclusion of the results and recommendations for future work.

2

Programme of Requirements

The goal of this program of requirements is to specify the features of the joystick that is to be developed. The purpose of the joystick is to demonstrate the operation and an application of 3D magnetic sensors. The joystick should function properly in a demonstration, whilst also remaining within the scope of the project. This is reflected in the requirements, which can be divided into functional, non-functional and trade-off requirements. Functional requirements state what the product must do and non-functional requirements state the qualities or attributes which the product must have. Lastly, for trade-off requirements, it is desired to comply as much as possible within the scope of the project.

2.1. Functional Requirements

1. The joystick design must be 3D printable.
2. Code that turns the detected magnetic fields into position must be developed.
3. Position measurement must be linked to a demonstration.
4. The joystick must be able to be calibrated.
5. An Arduino sensor readout interface must be developed for at least 2 commercial magnetic 3D Hall sensors.
6. There must be a validation process to check the angle error of the joystick.
7. The joystick must be able to work with at least one commercial magnetic 3D hall sensor.

2.2. Non-functional requirements

1. The joystick must use all 3 axes of the magnetic field in the 3D hall sensor detection.
2. The joystick must be able to rotate at least 61° from the z-axis in all 360°.
3. The joystick must have a resolution of at least 1° for both angles θ and ϕ as seen in Figure 1.4.
4. The joystick must have a minimum accuracy of 1° for both angles θ and ϕ.
5. The sensor electrical readout must not be saturated by the magnet at any point.
6. The latency of the entire system must be smaller than 30 ms.
7. The demonstration must have at least 60 frames per second.
8. The sensor output must have a first order relation to the angle of the joystick.

2.3. Trade-off requirements

1. The joystick should preferably work with as many sensors as possible.
2. The joystick should preferably have a mechanism that makes it return as close as possible to its zero position.
3. The signal to noise ratio at the output of the sensor should preferably be as high as possible.

2.4. Requirement Justification

The functional requirements are clearly defined by the bachelor project assignment. However, the non-functional requirements may require some clarification. All three axes of the magnetic field must be used, because the purpose of the project is to demonstrate a 3D magnetic sensor. Using only two axes of a 3D sensor would eliminate the need for a 3D Hall sensor. In order to make the three axes more accurate than just two, the joystick must bend up to 61°, which forms the next requirement. The reasoning behind both of these requirements is further explained in section 3.3.

The angular resolution must be small enough to give the user the illusion that there are infinitely many directions and speeds for the demonstration. Hence, a resolution of at least 1° was chosen. A similar argument can be made for the accuracy. Furthermore, saturation of the sensor readout due to magnetic fields that are too strong will lead to error in the demonstration and must be avoided.

The latency, or delay of the system must be smaller than 30 ms, as larger delays may lead to lesser perceived performance and discomfort in users [25]. Furthermore, the amount of frames per second (fps) determines the "smoothness" of the demonstration. Using 60 fps is sufficient to make a small game out of the demo, which may be desirable in future work.

Lastly, a first order relation between the sensor output and the angle of the joystick is desired, as it provides more simplicity and accuracy. As mathematical equations get more complex, approximations are used more often, which may affect the performance of the joystick.

3

Design process

In this chapter, the design process is described and design choices are justified. The design consists of multiple steps, which are depicted in Figure 3.1. Firstly, in section 3.1 a sensor readout using Arduino should be developed, ideally for all four commercial sensors. One of those is then selected to use for the rest of the design. Parallel to this, as described in section 3.3, the magnetic field of a permanent magnet at different distances is simulated. Based on those simulations, it can be seen how the magnet should ideally move relative to the sensor, and one of the many possible sensor-magnet joystick configurations can be selected. Once these tasks are finished, a magnet can be chosen. This is described in section 3.4. The section also describes how, based on the sensor, magnet strength and their configuration, the joystick can now be designed in SolidWorks and 3D printed. Finally, in section 3.5, an interface between Arduino and Python is created, such that the magnetic field can be converted into a position there. Putting everything together allows us to create an interactive demonstration, where a movement of the 3D printed joystick results in a moving dot on screen.

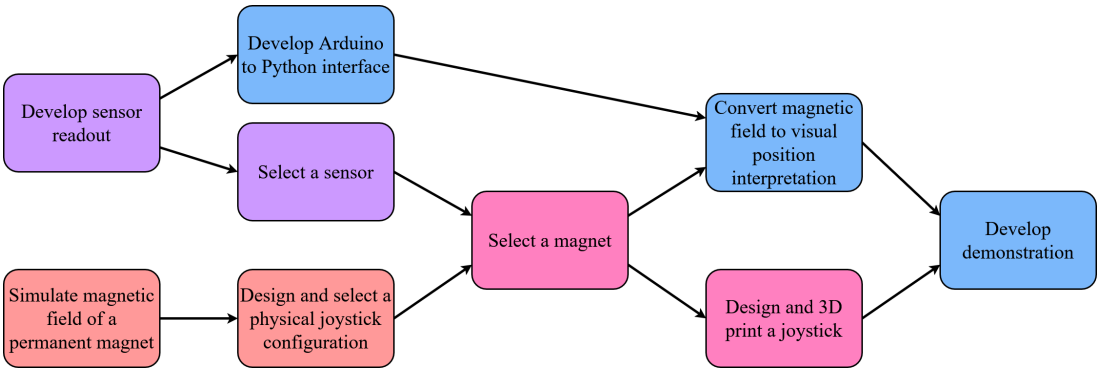

Figure 3.1: Design process. Each colour represents a section of this chapter.

3.1. Sensor readout

Four commercial 3D Hall sensors are chosen, and a readout system using Arduino must be developed for at least two, but preferably all of them. These four sensors are presented below, including their respective range, resolution and data sheet. Some of the information in the subsections about each specific sensor is based on the data sheets.

Table 3.1: Table of all four available 3D Hall sensors

Sensor	Company	Range [mT]	Resolution [μT/LSB]	Data sheet
ALS31313	Allegro	± 50	24.4	[26]
TLE493D-W2B6 A0	Infineon	± 160	65	[27]
MLX90393	Melexis	± 50	1.202 (xy) and 1.936 (z)	[28]
TMAG5173-Q1	Texas Instruments	± 40	1.22	[9]

All four sensors can use the Inter-Integrated Circuit (I^2C) communication protocol, which will be used for the communication between the Arduino and the sensor. The I^2C bus consists of two bidirectional lines: the Serial Data Line (SDA) and the Serial Clock Line (SCL). Both lines are open-drain and require pull-up resistors. The SCL line carries the clock signal generated by the master to synchronize data transfers, while the SDA line carries the actual data.

Each 3D Hall sensor connected to the I^2C bus has a unique 7-bit address, which allows the master to target specific devices when sending commands or reading data. This address can be fixed or programmable. In many sensor designs, the address is partially configurable via external voltage levels applied to dedicated address selection pins. Some sensors also support dynamic address assignment or configuration over I^2C, allowing greater flexibility in systems with multiple identical sensors. To perform a sensor readout, the master sends a start condition, followed by the address of the target sensor along with a read or write bit. If the sensor acknowledges the request, the master can then send write or read commands. With a write command, the master is able to set internal registers in the sensor to configure the correct mode of the sensor. A read command asks the sensor to send the data from an internal register, which is then read by the master. A full readout sequence would follow the following steps:

1. Send a START condition.
2. Begin transmission by sending the sensor's I^2C address with a write bit.
3. Send the register to be read.
4. Wait for the sensor to acknowledge (ACK).
5. Send a repeated START condition.
6. Send the sensor's I^2C address again, this time with a read bit.
7. Read one or more data bytes from the sensor.
8. Send ACK after each byte except the last one.
9. Send a STOP condition to end the transmission.

TMAG5173

The Texas Instruments sensor (TMAG5173) is able to give a reading in 16 bits per axis. For each axis, the readout is split into multiple registers, one most significant byte and one least significant byte, since one register is only 8 bits. To obtain a full measurement for one axis, the I^2C master must read both of these registers and combine the two 8-bit values to reconstruct the full 16-bit signed integer. This involves shifting the MSB by 8 bits and performing a bitwise OR with the LSB. The sensor uses two's complement format for encoding signed values, which allows representation of both positive and negative magnetic fields. The TMAG5173 also has a low noise mode. In this mode, the sensor averages the values over time, essentially applying a digital low-pass filter, reducing the RMS noise from 92μT to 16.75μT. This does decrease the bandwidth from 10kHz to 0.4 kHz, which makes the latency larger. However, the latency still stays below maximum requirement, so the noise reduction is worth it.

MLX90393

The magnetic field of the Melexis sensor can be read out in two bytes, which is done in a similar fashion as the Texas Instruments sensor. Both the analog gain and the resolution can be set by the user. Together, this gives some control over the sensitivity and range. The lower range of 50 mT was chosen, as this is closer to the range of the other sensors. If the sensors have a similar range and resolution, it is easier to implement multiple of them in the joystick demonstration.

ALS31313

The Allegro sensor provides the magnetic field in 12 bits per axis. I^2C communication is done in the same way as is with the TI (Texas Instruments) sensor. However, the register structure differs: each register is stored across four bytes instead of a single byte, as in the TI sensor.

TLE493D

The Infineon sensor also has 12 bits per axis, but uses a slightly different I^2C readout protocol. The sensor uses either a 1-byte I^2C or 2-byte protocol, which does not readily work with the wire library in Arduino. However, the company provides a sensor readout library that is meant for their own development boards, but should also work for an Arduino.

Sensor choice

The Texas Instruments sensor was chosen to use first in the joystick design, since it has the smallest sensor board and a correctly working readout. The size of the board the sensor is soldered to matters, because this allows for a greater range of motion in the joystick. This will be further discussed in section 3.4.

3.2. Position mapping

To ensure that the joystick functions correctly and delivers accurate positional feedback, it is crucial to select a magnet and sensor pair that are properly matched. This means either choosing a suitable magnet for a given Hall sensor or selecting a sensor that matches the characteristics of the chosen magnet. The goal is to ensure that the magnetic field experienced by the sensor falls within its optimal measurement range throughout the entire range of joystick motion. This is depicted in Figure 3.2.

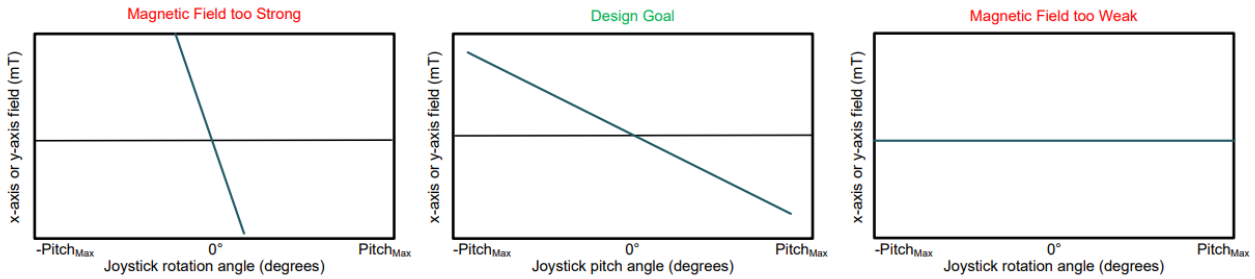

Figure 3.2: Sensor Design Goal [8]

A 3D Hall-effect sensor can be used to detect the precise position and movement of a joystick by measuring the magnetic field components (Bx, By, Bz) in three orthogonal directions. This setup typically involves attaching a permanent magnet to the moving part of the joystick, so that its motion relative to the fixed sensor produces varying magnetic field vectors. As the joystick is tilted or moved along the X, Y, or Z axes, the position of the magnet changes with respect to the sensor. This causes a corresponding change in the strength and direction of the magnetic field at the sensor location. This change in the magnetic field is a characteristic feature across all joystick designs that utilize a magnet and a 3D Hall sensor. Each specific mechanical configuration, whether the magnet is centred, offset, tilted, or mounted on a curved track, produces a distinct and repeatable relationship between the joystick position and the magnetic field vector detected by the sensor.

For a given design, the magnetic field at the sensor can be modelled as a function of the magnet's position and angle derived from the geometry of the joystick's movement. In most cases, the magnet follows an arc or spherical segment due to the pivoting motion of the joystick shaft. As a result, the magnetic field at the sensor can be expressed as a combination of translational and rotational contributions, where each component (Bx, By, Bz) changes smoothly as the joystick is tilted.

By characterizing this behaviour, either analytically or through simulation, it is possible to construct a forward model: a function that takes the joystick angle or deflection as input and outputs the expected magnetic field at the sensor. This is useful during design and simulation phases, allowing prediction of field strength limits, sensor saturation, and sensitivity regions. Importantly, this model can also be used in reverse. If the relationship between magnetic field and joystick position is predictable and behaves consistently, it becomes possible to infer the joystick's angular position directly from real-time magnetic field measurements. This reverse mapping, or inverse model, can be realized in several ways: through analytical equations, lookup tables derived from calibration data, or data-driven approaches such as machine learning.

In the implementations, this inverse approach enables the conversion of raw magnetic field components (Bx, By, Bz) into meaningful joystick outputs, such as angular positions or normalized X and Y positions. To maintain precision and responsiveness, the system could include additional processing steps such as linearization, temperature compensation, correction for sensor or magnet offsets, and filtering techniques that help reduce the effects of noise or mechanical variation.

3.3. Joystick configuration

This section explains the different configurations possible for the joystick. It goes into the characteristics of each design and explains the reasoning behind the chosen design. There are three different configuration types which all use a cylindrical magnet, but the magnet rotates around different points for each design. A cylindrical magnet was chosen because these types of magnets are widely available, easy to glue to a joystick and have a relatively straightforward magnetic field. A simple sketch of all designs is shown in Figure 3.3.

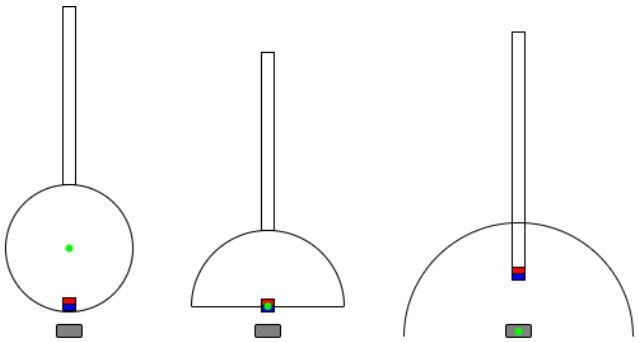

Figure 3.3: Three possible configurations of how the magnet moves relative to the sensor in a Hall effect joystick. The rotation centre point of the joystick is indicated in green, the magnet is red and blue and the sensor is indicated in grey.

Design 1 - Ball joint

The first design employs a ball joint mechanism, where a permanent magnet is embedded near the edge of a spherical ball, while the rotation point is located at the centre of the ball. As the joystick is manipulated, the ball pivots around its central point, causing the magnet to undergo angular displacement. This configuration introduces both rotational and translational components to the magnet's motion. While it primarily rotates, the distance between the magnet and the Hall sensor also varies due to the arc-like movement. This variation in distance between the magnet and sensor complicates the position mapping. Furthermore, the magnetic field is not uniform at the sensor and scales with a factor of $1/r^3$. As the joystick moves away from its neutral position, the distance between the magnet and the Hall sensor increases. Due to the inverse cubic relationship between magnetic field strength and distance from the source, this causes the magnetic field detected by the sensor to decay rapidly. As a result, the rate of change in the magnetic field becomes significantly smaller at larger deflections, leading to a reduced sensitivity in those outermost angular positions.

This behaviour may present a challenge in accurately detecting joystick movements near the extremes of its range. The loss of measurable magnetic gradient means that beyond a certain threshold, changes in joystick position produce minimal variation in sensor output, effectively compressing a wide range of physical motion into a narrow band of sensor response and thus increasing the sensitivity in that region. To better understand this phenomenon, the magnetic field distribution can be simulated using Python libraries such as MagPy. These simulations validate the theoretical expectation that the region near the neutral position contains most of the useful magnetic information, which can be seen in Figure 3.4. In practice, this means that a large portion of the sensor's dynamic range is concentrated around small displacements, which may require compensation techniques such as non-linear mapping or adaptive gain control to achieve uniform response across the entire motion range. Using a smaller range of motion, on the other hand, would significantly decrease the signal to noise ratio, which conflicts with the third trade-off requirement described in section 2.3

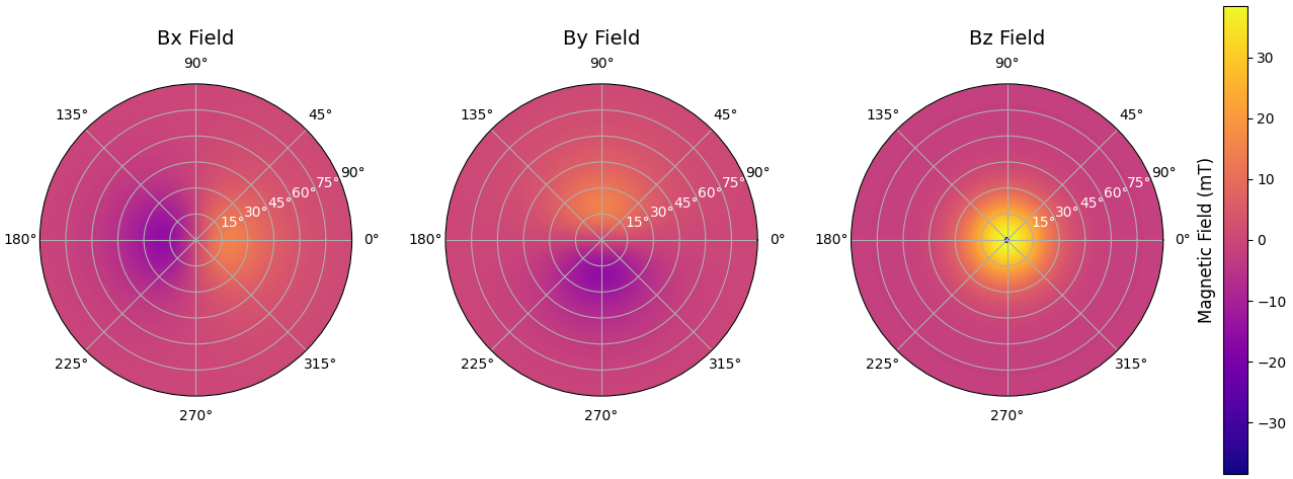

Figure 3.4: A simulation of the Bx, By, Bz magnetic fields observed by the sensor placed at (0,0) for different positions of a magnet, this holds for a magnet movement according to the ball joint design. θ of the magnet is shown from 0° till 90° radially and ϕ is shown for a full 360°.

Design 2 - Centred Magnet

The second design is similar to the first, in the sense that a magnet is placed on a moving ball. This time, however, it is not placed near the edge, but in the centre. This means that, as the stick moves, the centre of the magnet re-

mains stationary, resulting in a constant distance of the magnet to the sensor. This constant distance ensures that the magnetic field changes considerably less compared to a design where the magnet moves away. Regardless of the joystick's angle, the magnetic field signal will always be stronger than the noise if the distance is selected appropriately.

However, placing the sensor in close proximity to the magnet introduces a new set of challenges. At close range, the sensor no longer experiences a simple dipole field, but rather a highly non-uniform and spatially varying field that cannot be approximated as linear or symmetrical. Unlike at greater distances, where the magnetic field appears more uniform and predictable, the near-field geometry results in strong gradients and local field distortions. This non-uniformity complicates the process of mapping magnetic field readings to joystick angles. Small changes in angular position can produce non-linear and asymmetric variations in the sensor output, making calibration and interpolation more difficult. Additionally, the magnetic field may exhibit strong cross-axis coupling, where movement along one axis also influences readings on another, further complicating signal interpretation. Furthermore, since the magnet is very close to the sensor, its positioning is critical. If it is even slightly misplaced, this may result in a significant error at any angle. Hence, a design where the distance between the magnet and sensor is bigger, but still constant at every angle, may be preferred.

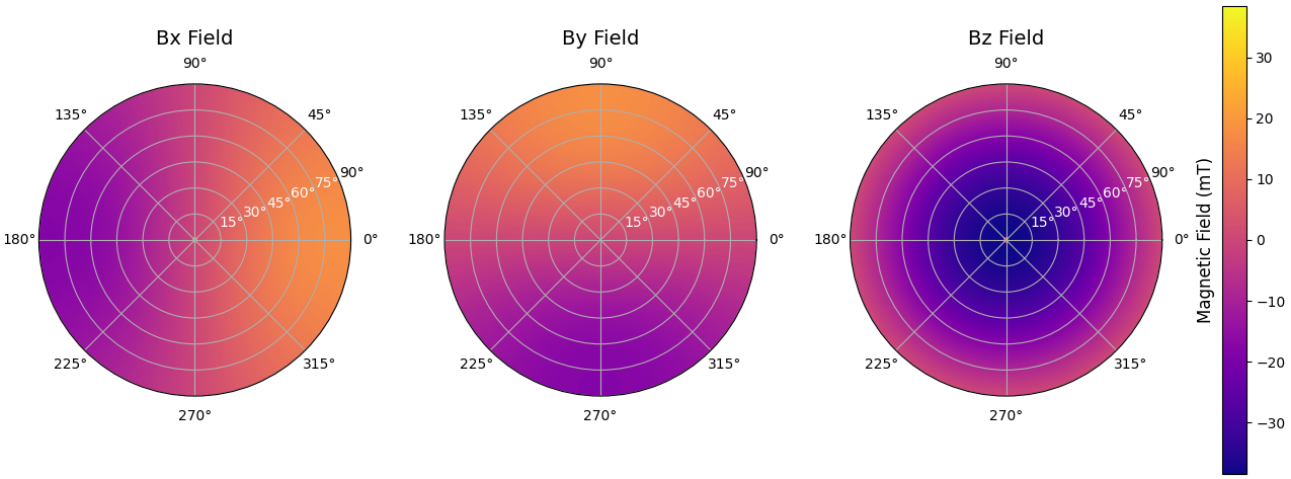

Figure 3.5: A simulation of the Bx, By, Bz magnetic fields observed by the sensor placed at (0,0) for different positions of a magnet, this holds for a magnet movement according to the centred magnet design. θ of the magnet is shown from 0° till 90° radially and ϕ is shown for a full 360°.

Design 3 - Centred Sensor

In contrast to the previous design, where the magnet remained stationary at the centre of rotation, this configuration places the Hall sensor at the centre, while the magnet moves along a spherical path above it. The distance between the sensor and the magnet remains constant, equal to the radius of the sphere defined by the magnet's path. Crucially, the magnet is oriented such that its magnetization axis always points toward the sensor. As the joystick moves, this alignment ensures that the sensor remains on the magnet's central axis. Consequently, the magnitude of the magnetic field detected by the sensor remains approximately constant, while only the direction of the field vector changes. Because the orientation of the magnetic field directly corresponds to the orientation of the joystick, the stick's angular position can be determined by analysing the direction of the measured magnetic vector. This allows for a straightforward and continuous mapping between sensor output and joystick position, using the following formulas:

$$\phi = arctan(\frac{H_y}{H_x}) \tag{3.1}$$

$$\theta = arctan(\frac{H_z}{\sqrt{H_x^2 + H_y^2}}) \tag{3.2}$$

This formula uses a fraction of the fields, rather than the absolute value of one of the fields. This could cancel some of the noise or temperature drift if the values are similar. However, since noise and drift are often additive, they can still affect the outcome of the formula. The simulations of the magnetic field change in this design can be seen in Figure 3.6.

Joystick design selection

In choosing a design, it is important to consider where the magnetic field changes the strongest. Stronger changes allow more precision in the measurements and a higher signal to noise ratio. For the ball joint design, the magnetic

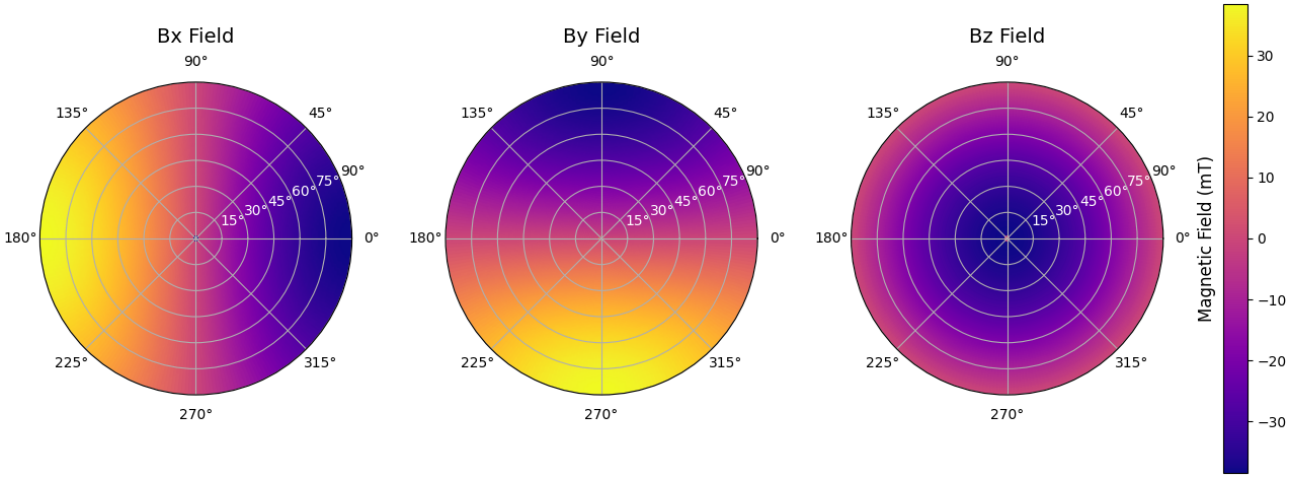

Figure 3.6: A simulation of the Bx, By, Bz magnetic fields observed by the sensor placed at (0,0) for different positions of a magnet, this holds for a magnet movement according to the centred sensor design. θ of the magnet is shown from 0° till 90° radially and ϕ is shown for a full 360°.

field fluctuates the most when the joystick is close to its zero position. Thus, this design is ideal when a smaller range of motion is required, with a small pitch angle θ. However, for this to work properly, the mechanics that make the joystick return to its zero position must be quite accurate. If the zero position is slightly off in this design, it could result in a large error. Designing an accurate return to zero mechanism is possible, but requires more mechanical engineering. Since this is an electrical engineering project, it was chosen to keep the return to zero mechanism simple. Furthermore, a slight misplacement of the magnet also results in a bigger error if a small range of motion is used. Hence, a bigger range of motion is better suited. The centred sensor design has its change in magnetic field spread out more evenly throughout the x and y components. The z component changes most strongly at the edge. Thus, it was chosen to continue with this design.

In order to get the most accurate measurements, the z field should be maximal at the zero position of the joystick. However, since the joystick will not bend 90 degrees, this means the x and y field will never reach their maximum, and thus the full range of the sensor will not be used. Instead, it is possible to discard the z field and set the x and y fields to their maxima at θ_{max}, extracting the position information from only the x and y fields. However, the purpose of this project is to demonstrate the working of a 3D Hall sensor, not a 2D Hall sensor. So the z field must stay. The fraction of the range that can be used in each field depends on the maximum pitch angle and is shown in Equation 3.3 and Equation 3.4.

$$R_z = \frac{1-\cos(\theta_{max})}{2} \tag{3.3}$$

$$R_{xy} = \sin(\theta_{max}) \tag{3.4}$$

So, in order to get the same or more information from all three fields rather than just x and y, these numbers together should be larger using the full range of only x and y. The full range corresponds to a relative range of 1, in two dimensions. So they must be larger than two.

$$\frac{1-\cos(\theta_{max})}{2} + 2\sin(\theta_{max}) > 2 \tag{3.5}$$

This yields that θ_{max} should be at least 61°. To conclude, in order to get more information from the three fields combined than one would get from just x and y scaled, the joystick must be able to bend up to at least 61 degrees. This conclusion leads to the second non-functional requirement, which is used to design the joystick in the next section.

3.4. Magnet choice, physical dimensions of joystick

Now that the path in which the magnet moves relative to the sensor is chosen, we can determine which magnet strength to pick, and what the dimensions of the design are. These choices are based on multiple requirements:

1. The joystick must be able to rotate at least 61° from the z-axis in all 360°.
2. The sensor must not be saturated by the magnet at any point.
3. The joystick should preferably work with as many sensors as possible.

There are multiple steps to the design of the joystick. Firstly, a sensor is selected based on its size and how well the readout performs. Next, a magnet is selected based on the magnetic range of this sensor. To have a higher signal to

noise ratio in the readout, ideally, we want to use a range that is close to the full range of the sensor. Furthermore, the distance to the sensor should be big enough to allow the magnet to move freely above the circuit board in the desired range of motion, but not too large, to prevent the joystick from getting really bulky. Another reason to have the distance bigger is that there will likely be some small alignment error in how the magnet is placed due to 3D printing. This alignment error is less noticeable in the magnetic field at the sensor if the magnet is further away. However, to use the full magnetic range of the sensor, the magnet needs to get stronger, and thus bigger, as it gets further away.

The Texas Instruments sensor has the smallest range of all four, so it is still possible to use other sensors in this range to meet the first trade-off requirement: the joystick should preferably work with as many sensors as time permits. We would like to use a big part of the 40 mT range of the Texas Instruments sensor, but without risking saturation. Hence, it is best to aim slightly below this, between 30 and 39 mT. To have a strong magnet that is not too heavy or big, it was chosen to use a neodymium magnet. This is the strongest material available to permanent magnets. A cylinder magnet with both a height and diameter of 6 mm was chosen. From simulations it followed that this magnet induces a magnetic field of approximately 39 mT when it is 10 mm away.

SolidWorks Joystick design

It is now known that the magnet should be at least 10 mm away from the sensor. A distance of 11 mm is chosen to account for 3D print tolerances or inaccuracies and avoid saturating the sensor. To make design 3 as described in section 3.2, the joystick consists of three parts: the stick, the middle part and the base. The base should have an elevated stand, which the sensor board can rest on such that its Hall plates are as close as possible the middle of the sphere the magnet traces out. Both the stick and the middle part should be big enough to move over this elevated stand, up to at least 61 degrees. To achieve this without making the design too bulky, the stick is bolted to the outside of the middle part. Furthermore, the middle part is made square such that it fits over the stand as far as possible. On the side where the stand protrudes more, it is built on a slight arc to give the middle part more range of motion. The design can be seen in Figure 3.7.

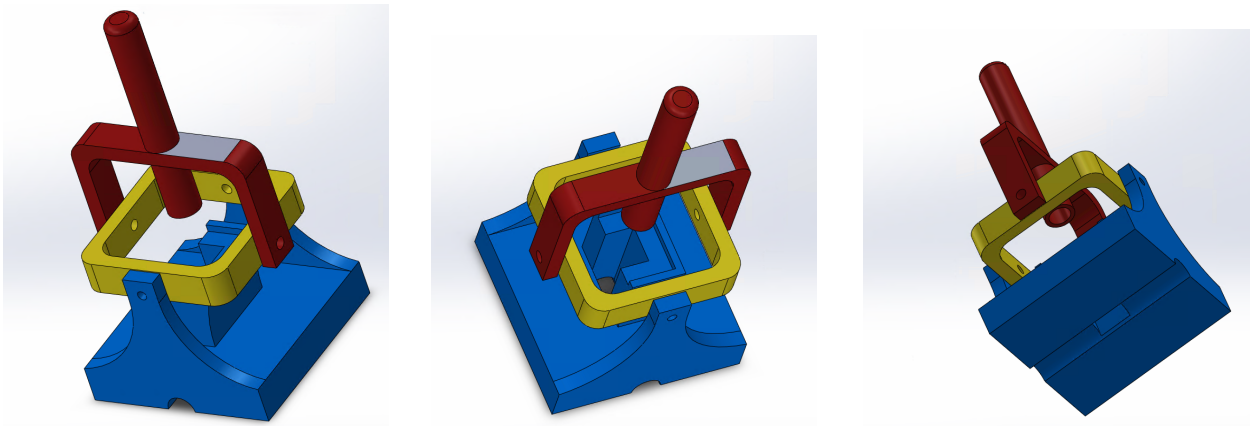

(a) (b) (c)

Figure 3.7: Solidworks joystick design at multiple angles. The stick is highlighted in red, the middle part in yellow and the base in blue.

The holes in the parts are where they will be screwed together once they are 3D printed. The size of the holes is chosen such that the screw will be stuck in the middle part, but loose on the stick and base. This way, the middle part and stick each move over a different axis, together allowing for the stick to move on a sphere. The magnet is attached to a hole inside the stick, positioned at the right distance of 11 mm from the sensor. The sensor holder platform and the bottom of the base both contain holes to allow wires to pass through, such that the sensor can be connected to the Arduino.

In order to allow movement up to 61 degrees, the screw in the base should be at a certain height. Since the angle is known, this height can be calculated using simple trigonometry. This is illustrated in Figure 3.8, and Equation 3.6 follows.

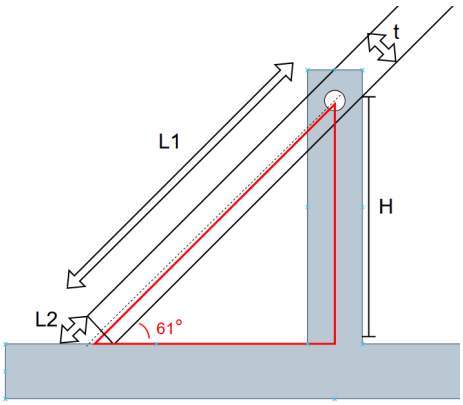

Figure 3.8: Calculation of base height

$$H = (L_1 + L_2) \sin(61°) \tag{3.6}$$

L_1 here is simply half the length of the middle part, but L_2 is a result of the angle and thickness of the middle part. Again using trigonometry, this is calculated as follows:

$$L_2 = \frac{t_{middle}}{2 \tan(61°)} \tag{3.7}$$

3.5. Demonstration

This section deals with the implementation of four functional requirements:

- Code that turns magnetic fields sensed in position must be developed.
- Position measurement must be linked to a demonstration.
- The joystick must be able to be calibrated.
- There must be a validation process to check the angle error of the joystick.

A visual demonstration on the computer screen was chosen, as this is more intuitive than just displaying numbers. To implement this easily, the Python library PyGame is used. This means, however, that the sensor readout data must be read from the Arduino by Python. Code for this is developed, and, using Equation 3.1 and Equation 3.2, the angles are then calculated. The angles are used for the demonstration and are compared with the physical angles for the validation process.

The demonstration is chosen to be a moving entity, which is a simple dot/ball, on a screen which movement is controlled by the joystick. The speed of the dot is determined by the pitch of the joystick, θ, and the direction of the movement corresponds to the rotation angle, ϕ. The speed of the dot is changed by moving the joystick away from or towards the centre, with the speed being zero when the stick is aligned on the z axis. This alignment, however, will not be very precise. A mechanical mechanism that makes the joystick return to its zero position will always have some error, which is why calibration is necessary. During calibration, the current measurement will be saved and considered the centre. Furthermore, a dead zone is implemented. A dead zone is a small area around the zero position where the output is set to zero to prevent the ball from moving around due to stray magnetic fields, noise or offset. The dead zone was chosen to be the circle where θ is smaller than or equal to 2°.

Given that the TI sensor outputs 16-bit data, the number of distinct values for θ is 2^{15}, as one bit is reserved for representing the negative values but θ is always positive. Applying Equation 3.2 and considering the smallest detectable change in H_x, with H_y and H_z remaining approximately constant, yields a minimum detectable variation in θ of 0.0017°. This value thus defines the resolution limit for θ. Similarly, applying Equation 3.1 to determine ϕ results in the same angular resolution of 0.0017°. In the context of the demonstration, this angular resolution corresponds to approximately $360°/0.0017° \approx 212{,}000$ discrete directions in which the ball can move. Assuming $H_y = 0$, each value of H_x corresponds to a unique H_z, implying that there are at least $2^{15} \cdot \sin(\theta_{\max}) \approx 28{,}700$ distinguishable values for θ, and consequently, distinct ball speeds. The range in ϕ can be expressed in θ, as seen in Figure 3.9. This shows that ϕ has a range of almost 200,000 steps at $\theta = 61$ °, close to its full range at $\theta = 90$ °.

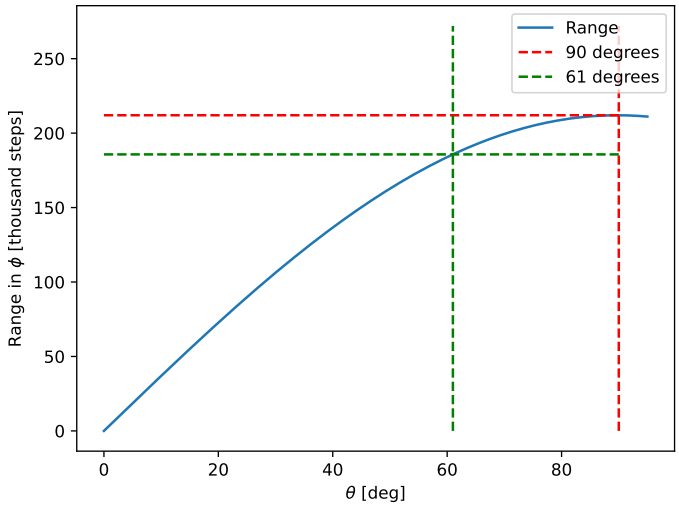

Figure 3.9: Range of ϕ expressed in θ, assuming the full magnetic range of 40 mT of the sensor is used.

Measurements and angle verification

Once the joystick is made, both the total strength of the magnetic field and the angle can be tested. The total strength of the field should be constant, so it can be calculated at multiple angles to see what the average total field is and its variance. Measurements are done at nine different angles: each corner, the middle points of the sides and the zero position.

The angle of the joystick can be approximately measured using a geometry triangle. This allows the verification of the second non-functional requirement: the joystick must be able to rotate at least 61° from the z-axis in all 360°. Furthermore, the measurements from the geometry triangle can be compared to the calculations based on the magnetic field measurement. This way, the angle error can be determined. The stick is kept at 90° compared to the x axis. While doing this, it can be held to the ground on one side, then halfway upward, and at the zero position. This is repeated on the other side, yielding five measurements where the stick is rotated around the x axis. Then, the stick is kept at 90° compared to the y axis, and the same procedure is repeated. To measure rotation angle ϕ, the square shape of the base can be used as a guide to hold the stick exactly above each of the four corners and in the middle of them. This yields eight measurements with 45° between them.

In order to improve the measurements, a guide was 3D printed. This guide consists of a dome that fits over the joystick. The dome has various holes at different angles, which the stick fits in. When the joystick is inserted in this dome, the angle of the stick is known based on the position of the hole. A circle with numerous holes for different angles ϕ is traced out for three angles of θ: 22.5°, 45° and 61°. For the circle at θ = 22.5°, a hole is placed at each 45° in ϕ. For both other circles at θ = 45° and 61°, ϕ takes steps of 22.5°. To better understand this configuration, the SolidWorks design of the dome is shown in Figure 3.10.

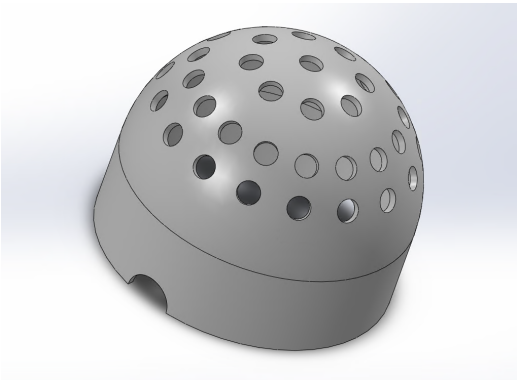

Figure 3.10: SolidWorks design of the dome

4

Prototype implementation and validation results

This chapter aims to present the results following from the design choices made in chapter 3. The final product consists of a joystick, where the magnet moves in a sphere with the sensor in the centre. This sensor is the TMAG5173 by Texas Instruments, which is connected to a laptop through an Arduino. The laptop runs a Python program, which takes the magnetic field data and turns it into a demonstration showing a moving ball and the position of the joystick.

4.1. Sensor Readout

The Arduino code for the sensors can be found in Appendix A. As described in the previous chapter, each sensor works slightly differently. Hence, different pieces of code were required. The Melexis and Texas Instruments sensors both measure a magnetic field that aligns with expectations in the presence of a magnet. The readout of the TI sensor can be seen in Figure 4.1. However, when the Texas Instruments sensor is held in a chamber with near zero magnetic field, it still measures a field of $(Bx, By, Bz) = (0.12, 0.24, 0.08)$ mT. Using Equation 3.2, this results in an angular offset with $\theta = 0.51°$ at the zero position of the joystick, where the magnetic field would theoretically be 30.2 mT in the z direction and zero in the other directions. The offset in θ is smaller than the dead-zone of 2°. Furthermore, it is still within the range given by the data sheet [9].

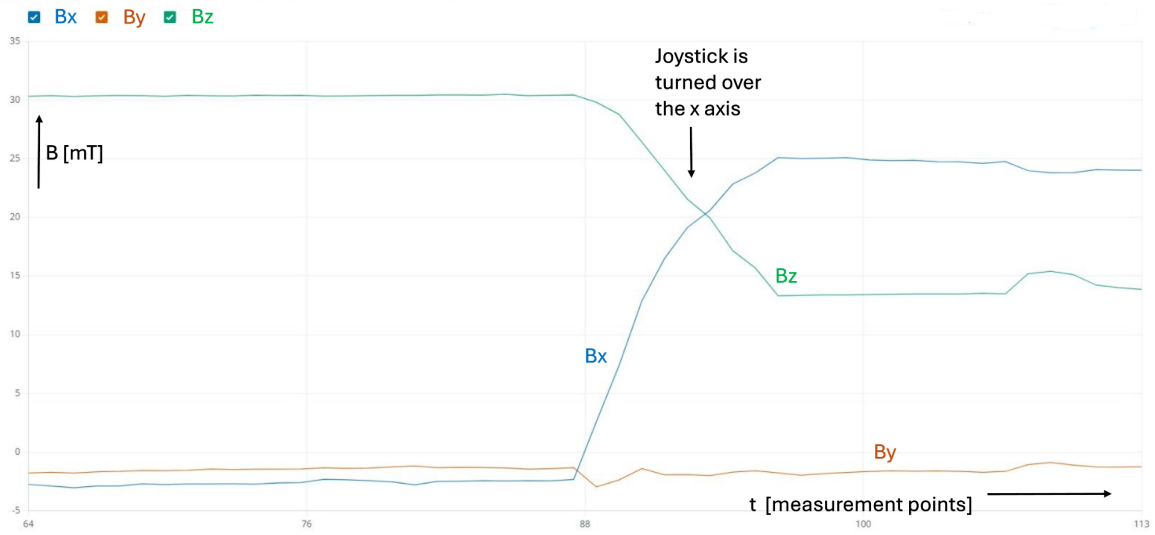

Figure 4.1: Arduino readout of the Texas Instruments 3D Hall sensor

The temperature sensor and magnetic field z component of the Allegro sensor work according to expectations. However, the x component of the magnetic field can only measure these four values: 0, -1, 15 and -16. While the I^2C protocol appears to work correctly, switching out the sensor for another one produces similar results. Because the z component and the temperature are working and by looking at the register mapping in Figure A.1, it is clear that the first two bytes are not being sent correctly by the sensor.
Infineon provides a library and example code to read out their 3D Hall sensor. However, this code reads out a constant value for the magnetic field, even when a magnet is moved near the sensor.

4.2. Joystick design

The 3D printed joystick can be seen in Figure 4.2. The base is 52 mm wide and 43 mm tall. The stick is 60 mm long, which makes the total height of the joystick in its zero position 106 mm. The distance between the sensor and the middle of the magnet is 11 mm.

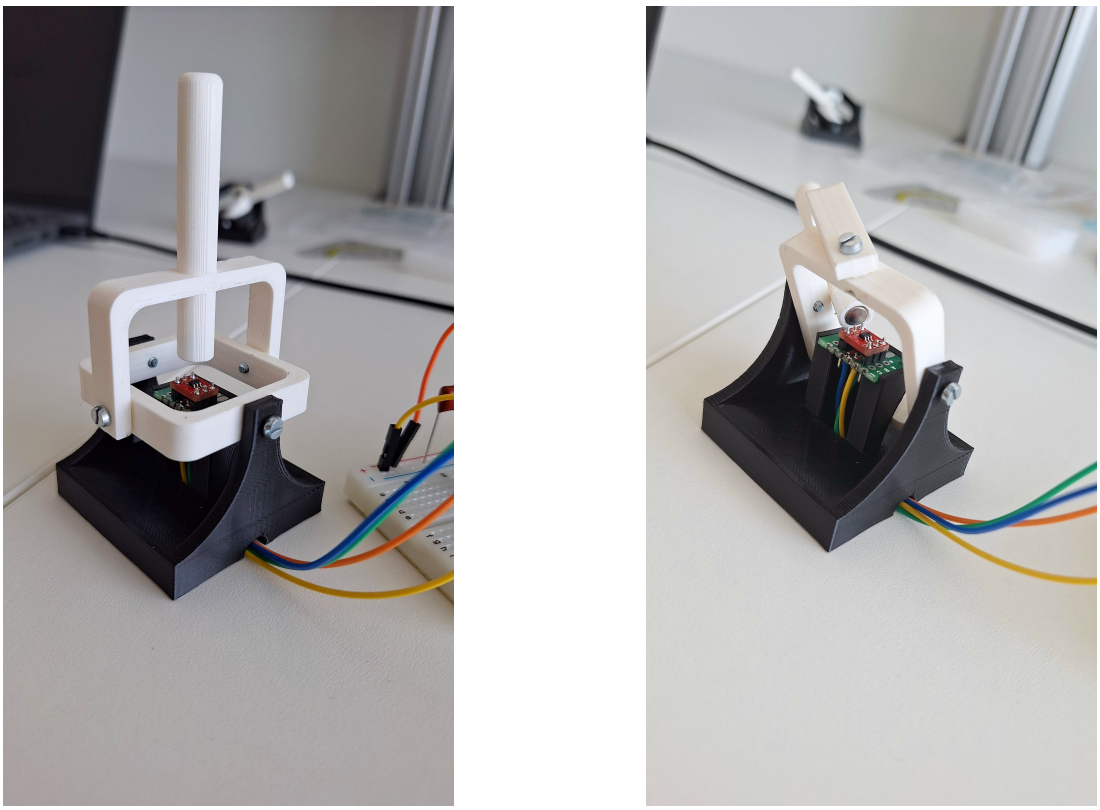

(a) (b)

Figure 4.2: Final 3D printed joystick with the magnet glued to the inside and the sensor mounted on the base.

Measuring the total magnetic field strength at different angles as described in section 3.5 yields the following average:

$$B_{total,average} = 30.2 \pm 0.8 \text{ [mT]} \tag{4.1}$$

The field fluctuates between approximately 27 and 34 mT, with a standard deviation of 2.3 mT.

4.3. Angle measurement

Both the pitch and the rotation angle of the joystick can be measured using the method described in section 3.5. The angles θ measured using the geometrical triangle versus those calculated using the magnetic field are shown in Table 4.1 for a rotation around the x axis and in Table 4.2 for a rotation around the y axis. The first and last measurements of each table were taken at the boundaries of the range of motion. Hence, they give an indication of the range of motion of θ around the x and y axes. Note that, by combining the ranges of motion of these axes, the stick can bend even further down to reach a bigger θ in the corners.

Table 4.1: θ measured by rotating around the x-axis

Measured	Calculated
62°	62°
28°	21°
0°	1.5°
40°	44°
60°	64°

Table 4.2: θ measured by rotating around the y-axis

Measured	Calculated
65°	68°
45°	48°
0°	1.3°
20°	22°
60°	63°

The rotation angle ϕ was also measured, at eight points. The square shape as the base is used as a guide for this. These measurements are presented in Table 4.3.

Table 4.3: Values of ϕ measured by comparing the position of the stick to the base versus calculated from the magnetic field

Measured	Calculated
-135°	-128.9°
-90°	-90.0°
-45°	-45.2°
0°	0.2°
45°	47.8°
90°	91.5°
135°	133.8°
180°	179.3°

Based on these tables, the mean error between the measured and calculated angles can be determined. This is 2.4° for θ and 1.59° for ϕ.
However, the 3D printed angle measurement guide also provides results. The calculated angle can be compared to the theoretical angle of the corresponding hole. Plots of the resulting error can be seen in Figure 4.3. Using this method, the mean absolute error is found to be 4.52° for θ and 5.05° for ϕ.

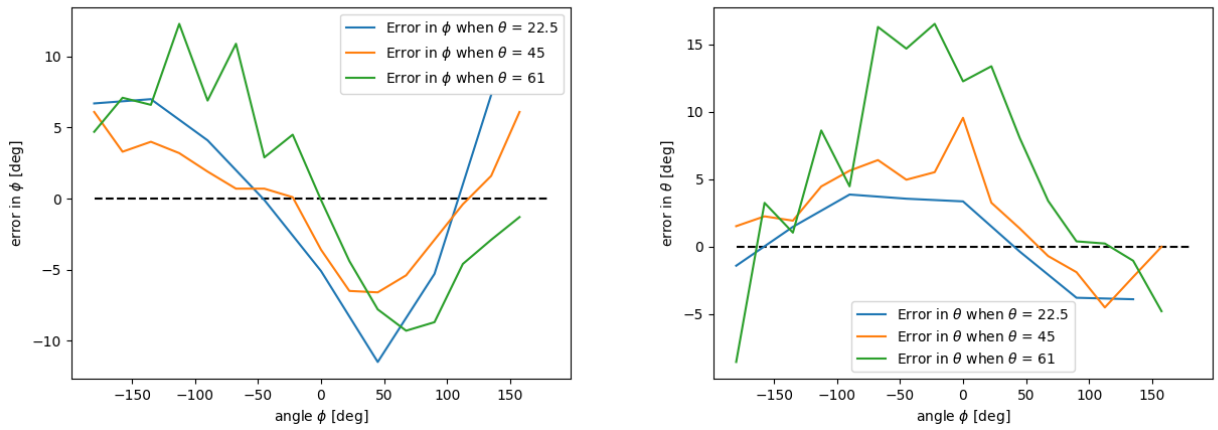

(a) Error in ϕ for varying values of ϕ and θ

(b) Error in θ for varying values of ϕ and θ

Figure 4.3: Plots of how the error in both angles changes with ϕ

4.4. Demonstration

The python code that was used to read out the Arduino, calculate the position and implement the demonstration can be found in Appendix A. The demonstration itself consists of a screen with a moving dot, which can be seen in Figure 4.4. The position of the joystick is also presented in a corner of the screen.

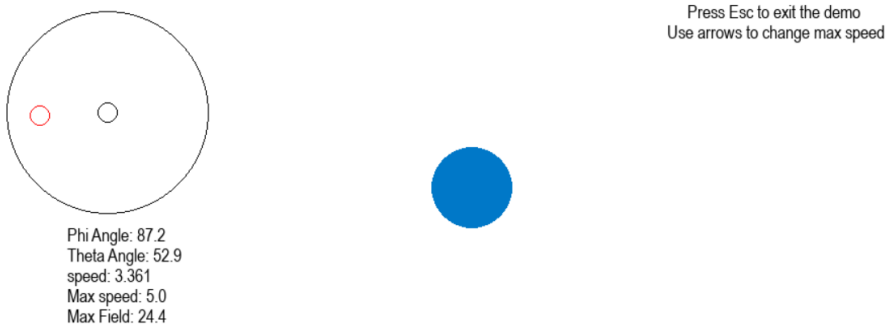

Figure 4.4: Visual demonstration consisting of a moving dot and the joystick position.

The total delay of the demonstration can also be approximated. The Texas Instruments sensor has a readout frequency of 400 Hz, which results in a maximum delay of 2.5 ms. The Arduino has a delay of 5 ms built in, which can be seen in the Texas Instruments code in Appendix A. If the demo has to be at least 60 frames per second, the maximum system latency must be lower than the time between each frame, 16 ms. The demonstration waits for the Arduino to send

new data before updating its frame. The demonstration generates 110 frames per second, resulting in a total delay of 9 ms.

The resolution in the demonstration can be derived from the average total magnetic field strength and the resolution of the sensor. Given that a range of ± 30.2 mT is used and the sensor has a resolution of 1.22 μT, there are 24,754 distinct values of the magnetic field per axis. However, because the joystick only bends up to approximately 61°, Equation 3.4 and Equation 3.3 must be used to calculate what fraction of these values can be used. This yields 21,650 possible values for both the x and y axis, and 6375 values for the z axis. Determining the exact amount of possible values for the angles from this and Equation 3.2 and Equation 3.1 requires more advanced mathematical reasoning, however, it can easily be seen that x and y will create at least 21,650 unique fractions together, and therefore at least 21,650 unique angles ϕ can be measured. Based on the magnetic field simulations for design 3, these angular positions should be relatively evenly spread over the 360°, meaning the resolution is higher than 1°. A similar argument can be made for θ, where each of the 6375 unique values for the z field should result in a unique value for θ. Figure 3.9 can also be used to determine the range of ϕ at θ = 61° by scaling the figure to take the range of 30.2 mT into account. This yields a range of 139,283 steps, which is much higher than the minimum range determined earlier.

5

Discussion

The validation of the angles of the joystick is not that precise. Measuring the angle with an protractor triangle is not easily done or precise and thus it is possible that the error in our measurement was bigger than the angle in the joystick. However, using the 3D printed dome to perform measurements leads to worse results, with a much bigger error. This can mean two things: either the position of the stick in the dome is very imprecise, or the joystick itself has a larger error than initially thought. By looking at Figure 4.3, a correlation between the errors can be seen, meaning that there is some sort of offset at play rather than random noise. This indicates that there may be an offset in the joystick. Since the working sensors have been characterized using a Helmholtz coil [29], we can check if this offset can be caused by the Texas Instruments sensor itself. A plot of the error in the sensor versus the joystick can be seen in Figure 5.1. By

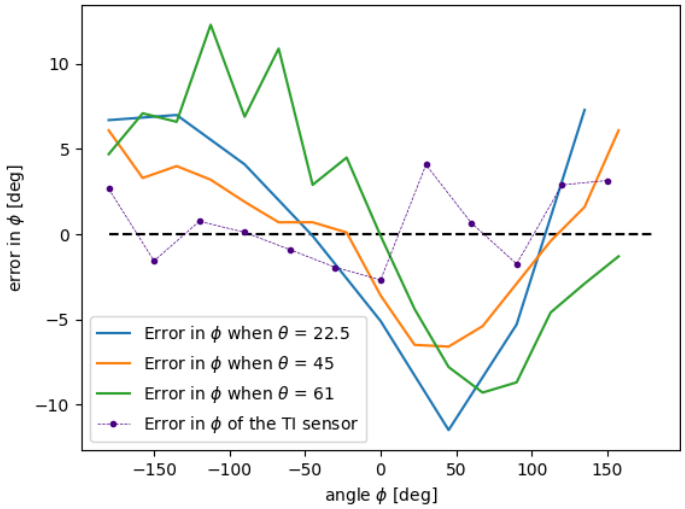

Figure 5.1: Comparison of the joystick error to the sensor error.

comparing the error trend of the joystick to that of the sensor, there does not seem to be a strong correlation. So it is more likely this offset is due to a physical misplacement. For example, if the sensor is not exactly in the midpoint of the movement but slightly on the left or right of it, this could result a larger ϕ on one side and a smaller ϕ on the other. Furthermore, the magnetization axis may not be perfectly in the centre of the magnet, which would result in a similar error.

While the latency can be estimated using the frames per second of the demonstration, it is not possible to have one answer on the exact latency of the total system. This latency is not only determined by the sensor and Arduino, but also by the computer that the demonstration is running on. The delay from the sensor and Arduino is always the same, so these give us the lowest possible latency, but the total system latency is determined by the hardware of the computer.

Since the Allegro sensor does not fully work, it is good to investigate what was working and which part did not work. As explained earlier, it was possible to read the 0-15 bits of a register. One might think that the first two bytes sent by the sensor, bits 16-31, are not read correctly by the Arduino. After connecting an I^2C analyser to the communication

lines, it was confirmed that the Arduino is reading the data correctly. This meant that the issue either has to be in the sensor, or a wrong read command is sent to the sensor, with the latter one being expected. It is remarkable that the issue is the same for both registers, since the read command asks the sensor to send 8 bytes at once starting from the address 0x28. This would send the 4 bytes from 0x28, followed by the next 4 bytes from 0x29. After spending quite some time on figuring out the problem and not being able to solve it, it was decided to move on to the other sensors.

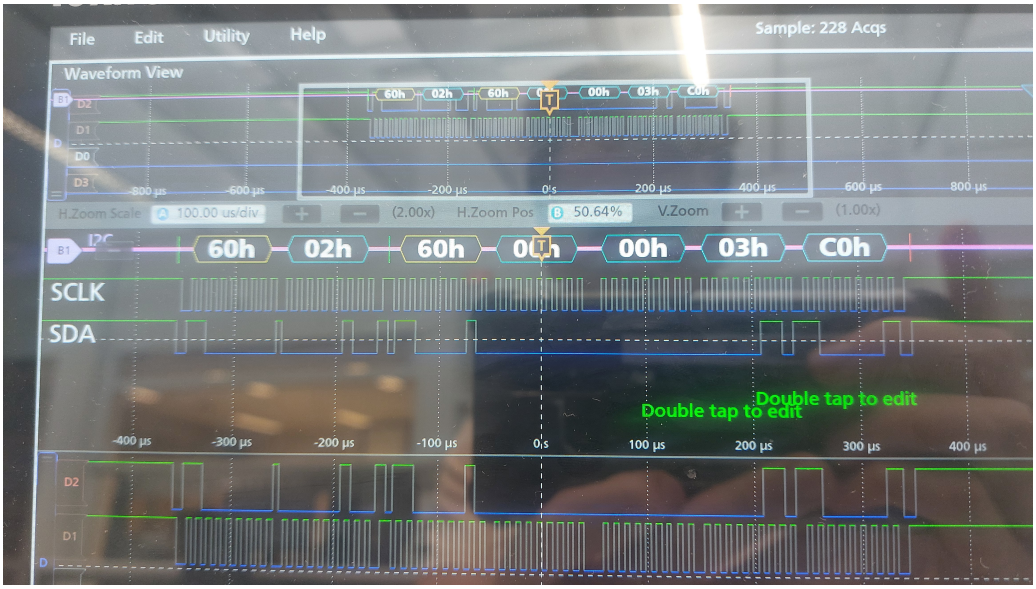

Figure 5.2: The readout of a digital analyser for the I^2C communication bus with the Arduino. In this case the content of register 2 is requested.

Another good point to address is the resolution. The sensor measures the x, y and z components of the field, which have a given resolution from the manufacturer. This does however not easily translate to a resolution for the joystick, in θ and ϕ. There is not one uniform resolution for either θ or ϕ, they both depend on the angle of the other. To explain this further for ϕ, we can take a θ close to 0. At the smallest deviation of θ from zero in the x and y direction one always has a ϕ of 45° no matter the resolution of the sensor, this would mean that the resolution at that point is 45°. When θ increases, then the amount of possible values for ϕ also increases. Hence, when θ is in its maximum, the resolution of ϕ is the best. The amount of information for θ depends on the derivative of the information from the x/y axis and the z-axis. The highest resolution lies on the point where the combination of both axes is at its maximum. Since the y/x axis has a cosine relation with the angle and the z axis has a sine relation, the combination of the derivative would be $\sin(\theta)\cos(\theta)$, this has its maximum at 45°. The best resolution is thus found at $\theta = 45°$. The resolution is hard to determine exactly, since the resolution in both angles fluctuates depending on the location. However, approximations suggest that the resolution in most locations is more than sufficient to fulfil the requirement of 1°.

6

Conclusion

In order to properly assess the performance of the joystick, it is necessary to reflect back on the programme of requirements. Based on the results, we can conclude that all functional requirements have been met. That is, the readout interface is completed for two 3D Hall sensors, one of which can be put in a 3D printed joystick. This joystick is linked to a demonstration that also shows the position and the angle of the joystick, and simple calibration scheme is implemented within this demonstration.

Next, the validation of the non-functional requirements must be evaluated. All three axes of the sensor are used, and since the maximum total field strength measured is 34 mT, none of them gets saturated by the magnet at any point. Furthermore, a resolution of more than 1° was achieved. By choosing the third design with the centred sensor, there is a first order relation between the magnetic fields and the angle of the joystick. The latency of the entire system is 9 ms based on the sensor, the Arduino and the demonstration, but may be more due to some other factors that were neglected. Assuming these factors would add up to 20 ms, this would still lead to a latency less than 30 ms, and the requirement is met.

The joystick should be able to move at least 61° from its zero position, so θ_{max} must be at least 61°. From Table 4.1 and Table 4.2, this requirement is met based on the calculated angle, but not met based on the measured angle in. However, as discussed earlier, the measured angle may not be very precise. Hence, it is plausible to assume that this requirement was (almost) met. When doing angle testing with the 3D printed dome, the joystick fit in all the holes, including the ones placed at $\theta = 61°$. So it can be concluded that this requirement is met. However, the accuracy for both angles is less than 1° in both measurement methods. Hence, the requirement to have an accuracy of 1° was unfortunately not met.

Lastly, trade-off requirements are discussed. As of now, the joystick only works with one sensor and does not have a return to zero mechanism. However, this can both be done in future work. The signal to noise ratio is made higher by activating the low-noise mode in the sensor, which averages the measured values before sending them. A stronger low-pass filter could be applied, however, this would negatively impact the delay of the sensor, and thus the latency of the system.

6.1. Future work and Recommendations

Whilst the joystick demonstrator lives up to most requirements, there are still many things that could be added or improved upon in future work. One of these is making the joystick such that it can be used with multiple sensors. Once the sensor readout is working correctly, bringing this output to the demonstration is easily done. However, the stand that holds the sensor inside the 3D printed joystick is specifically made for the Texas Instruments sensor. Ideally, this stand could be swapped out for another, such that the joystick is able to work with multiple 3D Hall sensors. Note that these sensors then must have a range of at least 34 mT, since they would saturate otherwise. In order to include sensors with a smaller measurement range, the magnet must be placed further away.

Many joysticks also employ a return to zero mechanism. This is often done using mechanical components underneath the stick. However, in this design, the sensor resides here, so another solution must be found. The simplest method to make the joystick return to its zero position consists of attaching springs or elastics between the parts. However, this may result in more error in the zero position, due to the springs not being exactly equal in strength.

The demonstration could also be made much more elaborate in future work. As of now, the demonstration consists of a moving ball, but this could be made into a game that uses the joystick as input. Since the demonstration

is already made using PyGame, this same library could easily be used to make a game. However, depending on the type of game, the latency may be more critical, and more attention should be spent on reducing the delay of the code. Other programming languages may be more suited to develop games that require very high fps.

The angle validation process can be improved. If the cause of the relatively big angular errors can be determined, appropriate measures can be taken. The error may be in the measurement method using 3D printed parts, in which case a more precise method must be used. The design of the 3D print can also be reconsidered.

Bibliography

[1] J. H. Choi, Y. Chung, and S. Oh, "Motion control of joystick interfaced electric wheelchair for improvement of safety and riding comfort," Mechatronics, vol. 59, pp. 104–114, 2019, ISSN: 0957-4158. DOI: https://doi.org/10.1016/j.mechatronics.2019.03.005. [Online]. Available: https://www.sciencedirect.com/science/article/pii/S0957415819300339.

[2] D.-H. Lee, "Operator-centric joystick mapping for intuitive manual operation of differential drive robots," Computers and Electrical Engineering, vol. 104, p. 108 427, 2022, ISSN: 0045-7906. DOI: https://doi.org/10.1016/j.compeleceng.2022.108427. [Online]. Available: https://www.sciencedirect.com/science/article/pii/S0045790622006449.

[3] Y. Ohmura, "6 - clinical application of soloassist, a joystick-guided robotic scope holder, in general surgery," in Handbook of Robotic and Image-Guided Surgery, M. H. Abedin-Nasab, Ed., Elsevier, 2020, pp. 89–105, ISBN: 978-0-12-814245-5. DOI: https://doi.org/10.1016/B978-0-12-814245-5.00006-2. [Online]. Available: https://www.sciencedirect.com/science/article/pii/B9780128142455000062.

[4] M. Hedegaard, N. Støttrup, F. F. Sørensen, T. H. Langer, and A. Samani, "Evaluation of five steering input devices in terms of muscle activity, upper body kinematics and steering performance during heavy machine simulator driving," International Journal of Industrial Ergonomics, vol. 72, pp. 137–145, 2019, ISSN: 0169-8141. DOI: https://doi.org/10.1016/j.ergon.2019.05.008. [Online]. Available: https://www.sciencedirect.com/science/article/pii/S0169814118301306.

[5] S. Campbell, How to use potentiometers on the arduino. [Online]. Available: https://www.circuitbasics.com/how-to-use-potentiometers-on-the-arduino/.

[6] Alps alpine's stick controllers (thumbpointer™), 2025. [Online]. Available: https://tech.alpsalpine.com/e/products/faq/muiti-control-device/thumbpointer/.

[7] Electronic waste (e-waste), Accessed: 01-06-2025, 2024. [Online]. Available: https://www.who.int/news-room/fact-sheets/detail/electronic-waste-(e-waste).

[8] S. B. Patrick Simmons, "Joystick and lever design with hall-effect sensors," 2023, Rev. A. [Online]. Available: https://www.ti.com/lit/ug/slyu064a/slyu064a.pdf.

[9] Low-power linear 3d hall-effect sensor with i2 c interface datasheet, TMAG5273, Rev. B, Texas Instruments, 2024. [Online]. Available: https://www.ti.com/lit/ds/symlink/tmag5273.pdf?ts=1745569337328&ref_url=https%253A%252F%252Fwww.ti.com%252Fproduct%252FTMAG5273.

[10] M. A. Khan, J. Sun, B. Li, A. Przybysz, and J. Kosel, "Magnetic sensors-a review and recent technologies," Engineering Research Express, vol. 3, no. 2, p. 022 005, Jun. 2021. DOI: 10.1088/2631-8695/ac0838. [Online]. Available: https://dx.doi.org/10.1088/2631-8695/ac0838.

[11] J. Lenz, "A review of magnetic sensors," Proceedings of the IEEE, vol. 78, no. 6, pp. 973–989, 1990. DOI: 10.1109/5.56910.

[12] P. R. (ed), "Magnetic sensors and magnetometers," Measurement Science and Technology, vol. 13, no. 4, p. 645, Apr. 2002. DOI: 10.1088/0957-0233/13/4/707. [Online]. Available: https://dx.doi.org/10.1088/0957-0233/13/4/707.

[13] J. S. Jacopo Ruggeri* and K. M. Dowling, "3d hall-effect magnetometer using a single inverted pyramid structure," IEEE 37th International Conference on Micro Electro Mechanical Systems (MEMS), 2024. DOI: 10.1109/MEMS58180.2024.10439529.

[14] S. Guo, "Integrated three-dimensional hall switch sensor based on independent optimized hall devices," Microelectronics Journal, vol. 135, p. 105 756, 2023, ISSN: 1879-2391. DOI: https://doi.org/10.1016/j.mejo.2023.105756. [Online]. Available: https://www.sciencedirect.com/science/article/pii/S0026269223000691.

[15] S. Guo, "Simulations of residual offset of five-contact vertical hall devices with slim waist," Solid-State Electronics, vol. 178, p. 107 986, 2021, ISSN: 0038-1101. DOI: https://doi.org/10.1016/j.sse.2021.107986. [Online]. Available: https://www.sciencedirect.com/science/article/pii/S0038110121000319.

[16] C. Wouters, V. Vranković, P. Chevtsov, and C. Hierold, "Calibration scheme for a new type of 3d hall sensor," Sensors and Actuators A: Physical, vol. 257, pp. 38–46, 2017, ISSN: 0924-4247. DOI: https://doi.org/10.1016/j.sna.2017.02.007. [Online]. Available: https://www.sciencedirect.com/science/article/pii/S0924424716307531.

[17] C. Sander, C. Leube, T. Aftab, P. Ruther, and O. Paul, "Monolithic isotropic 3d silicon hall sensor," Sensors and Actuators A: Physical, vol. 247, pp. 587–597, Aug. 2016, ISSN: 0924-4247. DOI: 10.1016/J.SNA.2016.06.038. [Online]. Available: https://www.sciencedirect.com/science/article/pii/S0924424716303260.

[18] C. Schott, J.-M. Waser, and R. Popovic, "Single-chip 3-d silicon hall sensor," Sensors and Actuators A: Physical, vol. 82, no. 1, pp. 167–173, 2000, ISSN: 0924-4247. DOI: https://doi.org/10.1016/S0924-4247(99)00331-3. [Online]. Available: https://www.sciencedirect.com/science/article/pii/S0924424799003313.

[19] H. K. Jacopo Ruggeri Udo Ausserlechner and K. M. Dowling, Inverted pyramid 3-axis silicon hall effect magnetic sensor with offset cancellation, 2024.

[20] S. Chikazumi and C. D. Graham Jr, "Ferromagnetism," in Physics of Ferromagnetism, Oxford University Press, Feb. 1997, ISBN: 9780198517764. DOI: 10.1093/oso/9780198517764.003.0006. eprint: https://academic.oup.com/book/0/chapter/422706899/chapter-pdf/52594633/isbn-9780198517764-book-part-6.pdf. [Online]. Available: https://doi.org/10.1093/oso/9780198517764.003.0006.

[21] W. AG, How do you calculate the magnetic flux density? [Online]. Available: https://www.supermagnete.nl/eng/faq/How-do-you-calculate-the-magnetic-flux-density.

[22] 0. S. 2021, A quick guide to magnets, magnetic metals & non-magnetic metals. [Online]. Available: https://www.eclipsemagnetics.com/resources/guides/a-quick-guide-to-magnets-magnetic-metals-and-non-magnetic-metals/.

[23] F. T. Ulaby and U. Ravaioli, Fundamentals of Applied Electromagnetics. Pearson, 2023.

[24] G. Alberts, H. Hollis, H. LaBollita, and G. Mueller, "On the sensitivity of a laser heterodyne polarimeter for vacuum birefringence detection," UF Journal of Undergraduate Research, vol. 20, no. 3, May 2019. DOI: 10.32473/ufjur.v20i3.106302.

[25] K. Brunnström, E. Dima, T. Qureshi, M. Johanson, M. Andersson, and M. Sjöström, "Latency impact on quality of experience in a virtual reality simulator for remote control of machines," Signal Processing: Image Communication, vol. 89, p. 116 005, 2020, ISSN: 0923-5965. DOI: https://doi.org/10.1016/j.image.2020.116005. [Online]. Available: https://www.sciencedirect.com/science/article/pii/S0923596520301648.

[26] Als31313, automotive grade, 3d linear hall-effect sensor with i2c output and advanced low power management, ALS31313, Accessed: 06-06-2025, Allegro Microsystems, 2021. [Online]. Available: https://www.allegromicro.com/~/media/Files/Datasheets/ALS31313-Datasheet.ashx.

[27] Low power 3d hall sensor with i2c interface and wake up function, TLE493D-W2B6 A0, Accessed: 06-06-2025, Infineon, 2019. [Online]. Available: https://www.infineon.com/cms/en/product/sensor/magnetic-sensors/magnetic-position-sensors/3d-magnetics/tle493d-w2b6-a0/.

[28] Mlx90393 triaxis® magnetic node datasheet, MLX90393, Accessed: 06-06-2025, Melexis, 2024. [Online]. Available: https://www.melexis.com/en/documents/documentation/datasheets/datasheet-mlx90393.

[29] A. Repriels and T. van Hooff, "A three dimensional automated testing platform for 3d magnetic sensors."

Appendices

A

Appendix

All Arduino code, Python code and SolidWorks files that were used in this project can be found on GitHub: `https://github.com/Tychobr/BAP`

A.1. Allegro Registers

0x28	X_Axis_MSBs								Y_Axis_MSBs								Z_Axis_MSBs								New Data	$\overline{\text{INT}}$	Temperature MSBs							
0x29	RESERVED											$\overline{\text{INT}}$ Write	X_Axis_LSBs				Y_Axis_LSBs				Z_Axis_LSBs				Hall Status		Temperature LSBs						
Address	31	30	29	28	27	26	25	24	23	22	21	20	19	18	17	16	15	14	13	12	11	10	9	8	7	6	5	4	3	2	1	0

Figure A.1: The register mapping of 0x28 and 0x29 for the Allegro sensor, containing the information of Bx, By and Bz